Structures 64 (2024) 106519

Contents lists available at ScienceDirect

Structures

journal homepage: www.elsevier.com/locate/structures

Accurate estimation of bearing capacity of stone columns reinforced: An investigation of different optimization algorithms

Hadi Fattahi [a], Hossein Ghaedi [a], Farshad Malekmahmoodi [a], Danial Jahed Armaghani [b,*]

[a] Faculty of Earth Sciences Engineering, Arak University of Technology, Arak, Iran
[b] School of Civil and Environmental Engineering, University of Technology Sydney, Sydney, NSW 2007, Australia

ARTICLE INFO

Keywords:
Geotechnical materials
Bearing capacity
Geogrid-reinforced stone columns
Optimization algorithms
Uncertainties

ABSTRACT

The precise estimation of bearing capacity (qrs) of stone columns reinforced with geogrid is crucial given the intricate nature of geotechnical materials and geological factors. However, the cost and complexity involved in determining qrs necessitate the use of a precise and consistent nonlinear equation suitable for diverse case studies. To address this, intelligent methods like nature-inspired optimization algorithms have emerged as effective solutions, enabling time and resource savings through accurate modeling. This research explores the utilization of two optimization algorithms, specifically Artificial Bee Colony (ABC) and Harmony Search (HS), for the estimation of qrs. Input parameters for modeling encompass the ratios of geogrid-reinforced layer diameter to footing diameter, GRSB and USB thickness to base diameter, unreinforced soft clay qrs, stone column length to diameter, and settlement to footing diameter. Finally, to assess the precision of the models, statistical indicators including Variance Account For (VAF), squared correlation coefficient (R^2), mean absolute percentage error (MAPE), mean square error (MSE), and root mean square error (RMSE) were computed. According to the findings of this study, the accuracy achieved by employing smart methods using the ABC algorithm ranged from 0.981 to 0.989, with error rates ranging from 7.86×10^{-5} to 0.00883. Similarly, the accuracy of the HS algorithm was determined to be between 0.984 and 0.988, with error rates ranging from 3×10^{-5} to 0.00551. These results underscore the high accuracy of intelligent algorithms, offering a dependable means of determining qrs across various study areas while considering uncertainties.

1. Introduction

Excessive settlement and tilting are common challenges faced by structures built on soft clay, often due to soil shear failure. One effective remedial measure is the installation of stone columns beneath the footing. When loaded, the stone columns expand and displace the surrounding soil in all directions. However, the surrounding soil restrains the stone columns within their immediate vicinity, allowing them to bear vertical loads. The application of geosynthetics to each stone column enhances the load-carrying capacity of the columns by increasing confinement. The encasement prevents the stones from penetrating the surrounding clay, thereby increasing the soil's load-qrs and rigidity, while reducing settling and deformation [1–13]. Over the past three decades, numerous studies have been conducted to investigate the bearing capacity (qrs) of stone columns reinforced with geogrid. The objective of these investigations was to deepen our comprehension of how the ground behaves and performs when stone columns are employed [14–19]. Another research conducted by Murugesan and Rajagopal [20] and Lo, Zhang [21] focused on stone columns with vertical covers using numerical methods. Their findings indicated that limiting the bulging of stone columns can further enhance their load-carrying capacity and minimize settling. Moreover, Shahu and Reddy [22] investigated various factors influencing the qrs and settlement of stone columns through finite element analysis and a series of small-scale experiments. Additionally, Han and Gabr [23] conducted a numerical analysis that focused on ground platforms supported by piles and investigated their reinforcement with geosynthetics in soft soil. The study delved into the structural behavior and performance of these ground platforms, providing insights into the effectiveness of geosynthetic reinforcement in mitigating the challenges posed by soft soil conditions. Arulrajah, Abdullah [22] focused on utilizing a geogrid-soil platform that was supported by stone columns in a real railway project in Malaysia. Mehrannia, Nazariafshar [23] conducted extensive laboratory testing to evaluate the strength of stone columns and granular

* Corresponding author.
E-mail address: danial.jahedarmaghani@uts.edu.au (D.J. Armaghani).

https://doi.org/10.1016/j.istruc.2024.106519
Received 18 January 2024; Received in revised form 13 April 2024; Accepted 30 April 2024
Available online 14 May 2024

blankets in both reinforced and non-reinforced states. Andreou and Papadopoulos [24] investigated the variables influencing settlement assessment in stone column reinforced soils. Nav et al. [27] employed Abaqus numerical software to assess the mechanical characteristics of both regular and reinforced stone columns in soft soils. The findings of their study revealed that while columns alone can reduce soil settlements, the use of geosynthetics can further enhance these benefits. Xu, Moayedi [25] investigated the stress-strain behavior of reinforced (coated) and unreinforced (non-coated) stone columns for soft and weak soils. They employed finite element modeling software and experimental methods to examine the effects of dimensions, length, and other key factors. The study focused on geogrid-covered stone columns, settlement evaluation, and the influence of overhang on their effectiveness. Bazzazian Bonab, Lajevardi [26] conducted small-scale laboratory tests on reinforced floating stone columns to evaluate the impact of various geotextile placements, column diameters, reinforcement lengths, and reinforcement spacing. The findings indicated that the vertical casing stone column's cover advantage decreases with increasing diameter, while the performance of horizontal and vertical-horizontal cover stone columns improves. Moreover, vertical-horizontal composite stone columns exhibited significantly higher load-qrs compared to other types. Nazariafshar et al. [30] performed laboratory experiments to assess the load-qrs in geogrid-reinforced stone columns with granular blankets designed for flotation. They incorporated geosynthetic reinforcements, specifically geogrid and geotextile, to strengthen the stone columns and blankets, respectively. The study aimed to assess the impact of these geosynthetic reinforcements on the load- qrs of the system.Thakur, Rawat [27] performed a comparative study using Plaxis 2D and 3D software to examine the suitability of enclosed horizontal reinforced stone columns and stone pillars. The finite element analysis results showed that reinforced stone columns have higher qrs than unreinforced stone columns, both exhibiting buckling failure. The experimental approach was used to validate the results, which aligned well within an acceptable range of variation. Nasiri and Hajiazizi [28] discussed the results of triaxial tests conducted on reinforced stone columns using geotextile and geogrid enclosures. Hataf, Nabipour [29] investigated the impact of cover type, aggregate materials, and length on the qrs in dry sand and clay beds using PLAXIS^{2D} numerical software. Nayak et al. [34] investigated the impact of column arrangement on the effectiveness of stone columns installed in lithomargic clay and protected with geogrid, utilizing numerical software for analysis. Das and Dey [30] conducted research aiming to enhance the capacity of stone columns by utilizing a soil-cement bed stabilized on top of the stone column. Kardgar [31] employed PLAXIS numerical software to simulate the impact of stone columns on the load-qrs of clay soils. They concluded that the stiffness, length, and coverage of stone columns are crucial factors influencing their resistance, which should be considered in the analysis. Naderi, Asakereh [32] investigated the effect of stone column presence and placement on the qrs of a strip foundation adjacent to a soft clay slope using model testing and numerical modeling. In another study, Das and Dey [33] employed numerical analysis using Plaxis^{2D} software to observe the behavior of stone columns under a soil-cement bed (SCB) and regular stone columns (OSC) to increase their load-qrs. The obtained results were compared and confirmed through a limited number of laboratory studies. Pandey, Rajesh [34] utilized numerical software to examine embankments constructed on very soft soil and supported by stone columns covered with geogrid. Das and Dey [35] conducted laboratory studies on individual and grouped stone columns with and without soil-cement bases. The experimental data were compared with numerical results from ABAQUS^{3D}, revealing a strong correlation between them. Shafiqu and Al-Assady [36] performed a numerical analysis of a synthetically coated stone column embankment. Gu et al. [42] utilized the discrete element method (DEM) to comprehensively examine the influence of geogrid coverage on the behavior of soft clay when reinforced with stone columns. The research employed DEM to simulate and analyze the intricate interactions within the composite system, shedding light on the effects of geogrid reinforcement on the mechanical properties and performance of soft clay enhanced with stone columns. Vibhoosha et al. [43] investigated how the stiffness of geosynthetic material influences the behavior of stone columns within lithomargic clay. Prasad and Satyanarayana [44] conducted a comparison between plain reinforced stone columns and end-stone columns with geotextile covers made of silicon-manganese slag in soft marine clay. Yoo [45] presented the results of a numerical analysis on the load-qrs in geogrid-reinforced stone columns as foundation load-bearing elements. Fattah [46] explored the potential enhancement of soft clays using end stone columns with geogrid. Xie, Gao [37] conducted laboratory model testing on floating and end geosynthetic encased stone columns (GESCs) with different cover materials to evaluate their load-bearing performance under static stress. Deb, Samadhiya [38] reported the results of laboratory model experiments on a sand substrate without reinforcement and a geogrid-reinforced stone column system on soft clay. Li, Rajesh [39] studied the deformation behavior of geosynthetically coated stone columns in an undrained state using centrifuge model testing. Mazumder and Ayothiraman [40] employed finite element modeling (with Plaxis^{3D} software) to numerically analyze the behavior of conventional and restricted columns composed of various combinations of crushed rock aggregates and tire shredded chips.

While previous research has been valuable, conventional experimental, regression, analytical, and numerical methods often struggle to precisely determine the qrs due to their nonlinear and complex relationship with influencing variables. Therefore, intelligent methods, facilitated by advancements in computer science, offer a promising tool for accurately approximating the nonlinear function in complex engineering systems. For instance, Kuo, Jaksa [41] employed the Artificial Neural Network (ANN) technique to forecast and assess the bearing capacity of strip foundations and stone columns within multi-layered cohesive soil. Momeni, Nazir [42] predicted pile bearing capacities utilizing ANNs coupled with Genetic Algorithms. Their investigations revealed that employing ANN with Genetic Algorithms yielded superior performance in estimating pile and stone column bearing capacities compared to traditional ANN methods. Chik and Aljanabi [43] utilized Multilayer Perceptron (MLP) ANNs to estimate embankment settlement based on stone columns. Their analysis demonstrated the efficacy of MLP-ANN in modeling settlement accurately. Aljanabi, Chik [44] utilized Support Vector Machine (SVM), a soft computing technique, to predict stone column capacities. Statistical analyses indicated minimal errors associated with the employed technique. Mosallanezhad and Moayedi [45] employed a hybrid ANN model to estimate screw pile uplift resistance. Their model outputs highlighted the hybrid ANN's efficacy in predicting pile capacities robustly. Sahu, Patra [46] estimated strip foundation bearing capacities on reinforced soil using ANN techniques, concluding that their developed equation exhibited strong performance. Moayedi and Rezaei [47] utilized ANN methods to establish a straightforward and practical relationship for predicting stone column bearing capacities. Their proposed method demonstrated high accuracy, with a mean absolute error (MAE) of less than 0.262. Das and Dey [48] explored three Adaptive Neuro-Fuzzy Inference System (ANFIS) models, namely ANFIS-E with solely experimental data, ANFIS-A with analytical or numerical data, and ANFIS-EA with both experimental and analytical/numerical results, to investigate stone column bearing capacity behaviors. Their findings indicated that the ANFIS-EA model yielded the most favorable results among the tested models. Additionally, Das and Dey [49] employed Support Vector Regression (SVR) and ANN techniques to determine stone column final bearing capacities. Their results favored SVR for its superior predictive performance over ANN. Dey and Debnath [50] employed SVR-ERBF, SVR-POLY, and SVR-RBF models to forecast the bearing capacity of a sand bed reinforced with geogrid. Among the models developed, the SVR-ERBF model exhibited the least error. Mazumder and Garg [51] utilized linear regression, SVM, Gaussian Process Regression (GPR), and ANN techniques in MATLAB to estimate the radial strain and bearing

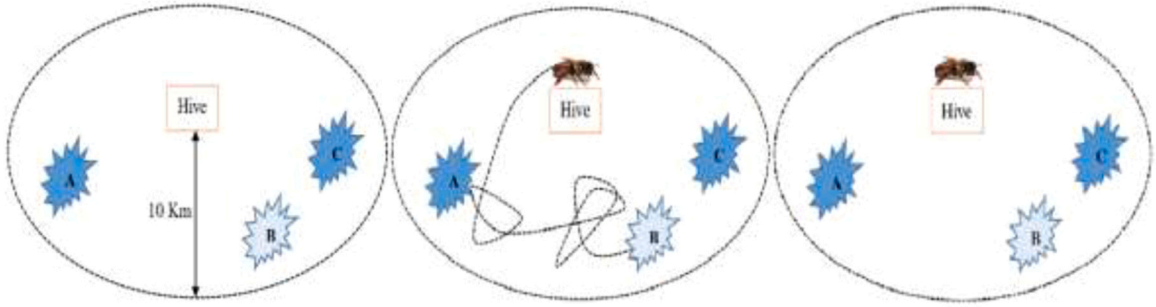

Fig. 1. illustrates a bee searching for flower patches [61].

capacity of stone columns. Their analysis indicated that the ANN technique yielded superior accuracy in model prediction. Moayedi and Hayati [52] utilized soft computing methods, including time-delay neural networks (FTDNN) and feed-forward neural networks (FFNN), to predict the load settlement response of piles and drilling columns. Their study concluded that the developed model, based on the proposed Cone Penetration Test (CPT), holds promise for predicting load transfer and settlement for single piles under axial load. Jahed Armaghani, Shoib [53] investigated the combined ANN model with the Particle Swarm Optimization (PSO) algorithm to estimate the bearing load of socketed piles. Bagińska and Srokosz [54] employed a Deep Neural Networks (DNN) model to predict the ultimate bearing capacity of shallow columns, demonstrating its suitability in handling large datasets. Sethy, Patra [55] predicted the bearing capacity of circular foundations on a layer of sand using the ANN technique, highlighting the model's high capability in operational design. Ardakani, Dinarvand [56] estimated stone columns enclosed with geotextiles using ANNs optimized with the Colonial Competitive Algorithm (ANN-ICA), showcasing the superiority of the ANN-ICA method compared to other ANN methods. Ghanizadeh, Ghanizadeh [57] utilized Multivariate Adaptive Regression Splines (MARS) and Escaping Bird Search Optimization Algorithm (EBS) to develop a model for predicting the bearing capacity of stone columns reinforced with geogrid. Their parameter analysis revealed that increasing all input parameters augments the bearing capacity. Gnanandarao, Onyelowe [58] employed an ANN technique to predict the bearing capacity of reinforced stone columns in soft soils. Lafifi, Rouaiguia [59] utilized Response Surface Method (RSM) and ANN techniques to optimize and estimate parameters affecting the bearing capacity of a shallow square foundation on sandy soil reinforced with geosynthetics. They also employed a multi-objective genetic algorithm (MOGA) in conjunction with RSM and ANN models to solve multi-objective optimization problems. Zeini, Lwti [60] estimated the bearing capacity of a sand bed reinforced with geogrid. They employed machine learning techniques including Multivariate Polynomial Regression (MPR), Random Forest (RF), and Linear Regression (LR), with statistical indicators indicating better performance of the proposed new Random Forest model.

In this paper, considering the numerous input parameters and the complexity of the model, intelligent methods replace experimental, analytical, regression, and numerical approaches to estimate the qrs, resulting in a significantly higher accuracy of the developed model. A nonlinear and complex relationship is employed for all case studies to account for uncertainty. In this study, a total of 219 samples were used, incorporating significant input parameters (5 input parameters) that directly influence the estimated qrs. The relationship established in this paper can serve as an efficient and practical model that can be applied to similar case studies and various drilling purposes. This holds particular significance because it accounts for the inclusion of multiple parameters that exert a substantial influence on the accuracy and efficacy of the model.

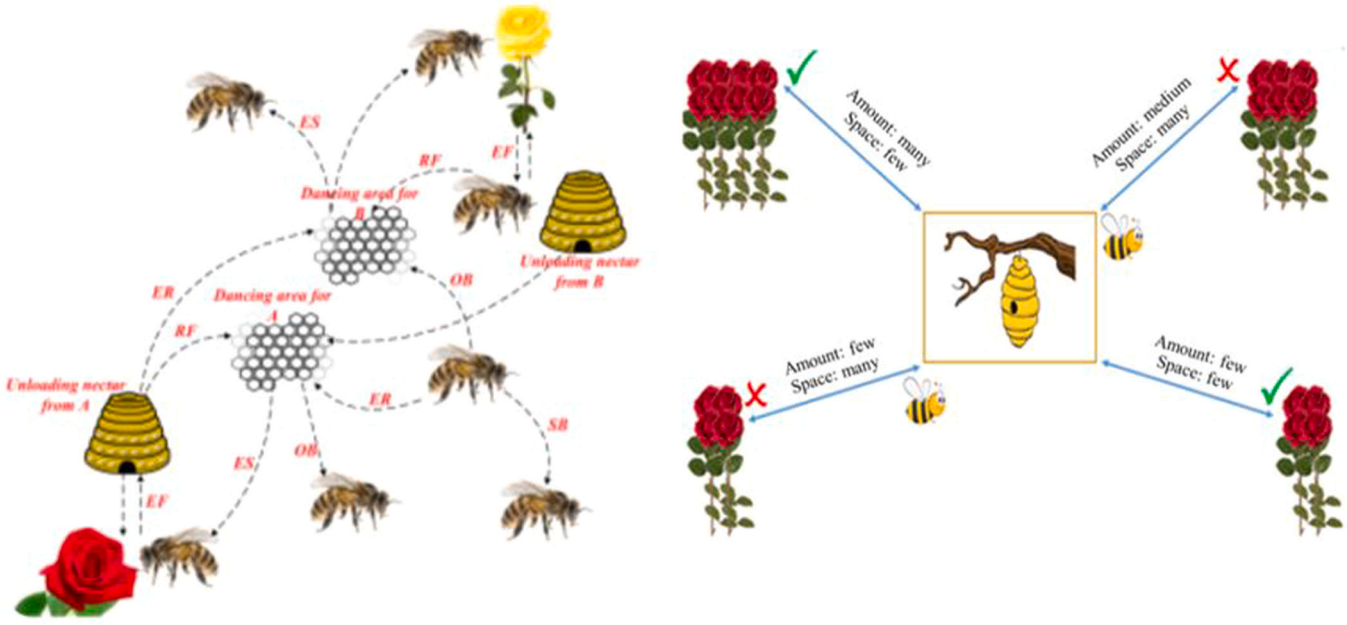

Fig. 2. demonstrates this optimal search behavior [61].

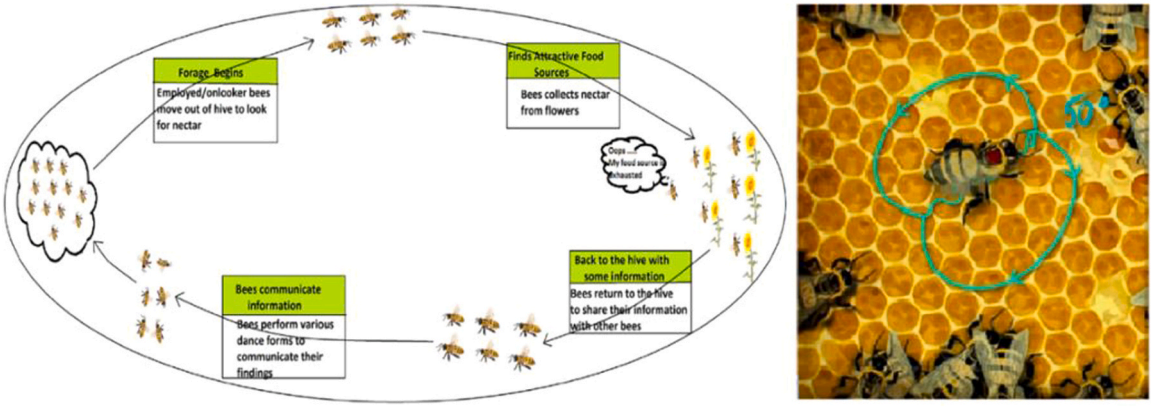

Fig. 3. The dancing bees and their sophisticated communication system for sharing information about food sources [61].

2. Intelligent methods used in this research

2.1. Artificial bee colony algorithm (ABC)

The ABC is an optimization algorithm designed to address optimization problems, drawing inspiration from the inherent behaviors of organisms and the observed physical laws in nature. Introduced by Karaboga in 2005 [51], the algorithm establishes a correlation between the number of bees in a hive and the initial count of potential solutions (food sources) within the search space of the optimization problem. Every food source represents a potential solution, and its quality, evaluated through the fitness level, is determined by the objective function of the given problem. The subsequent sections briefly delve into the dynamics of the bee colony, the foraging behaviors of bees, and provide an overview of the bee algorithm.

2.1.1. Bee colonies

A honey bee colony has the ability to disperse over long distances and explore various directions to exploit food sources. Bees tend to visit flower patches that offer abundant nectar and pollen, while avoiding areas with scarce resources.

In a bee colony, there are three main components: food sources, worker bees, and non-worker bees. Worker bees directly interact with the food sources from which they collect nectar. Additionally, bees within the hive communicate crucial information about the location, direction, and profitability of these food sources to their fellow hive members. Non-worker bees constantly search for new food sources, with scouts exploring the environment and observers receiving information from worker bees.

2.1.2. Search for food in nature

The process of searching for food in a bee colony begins with worker bees being sent out to search for promising flower patches that are rich in nectar or pollen. The worker bees randomly move from one flower patch to another, aiming to find the shortest and most rewarding path through the network of flowers. They optimize their search by seeking the shortest path and visiting patches with a higher density of flowers.

During the foraging season, the colony assigns sentinel bees to stay on alert and continue the search for food sources. Each sentinel bee performs a specific dance, known as the waggle dance, once it has completed the exploration of all flower patches. The waggle dance conveys information about the orientation of the flower patch relative to the hive, its distance, and its condition. Based on this information, other bees in the colony, known as follower bees, decide which flower patches to visit. Follower bees disperse randomly within the selected flower patch based on the information received from the waggle dance. Fig. 3 illustrates the dancing bees and their sophisticated communication system for sharing information about food sources [52].

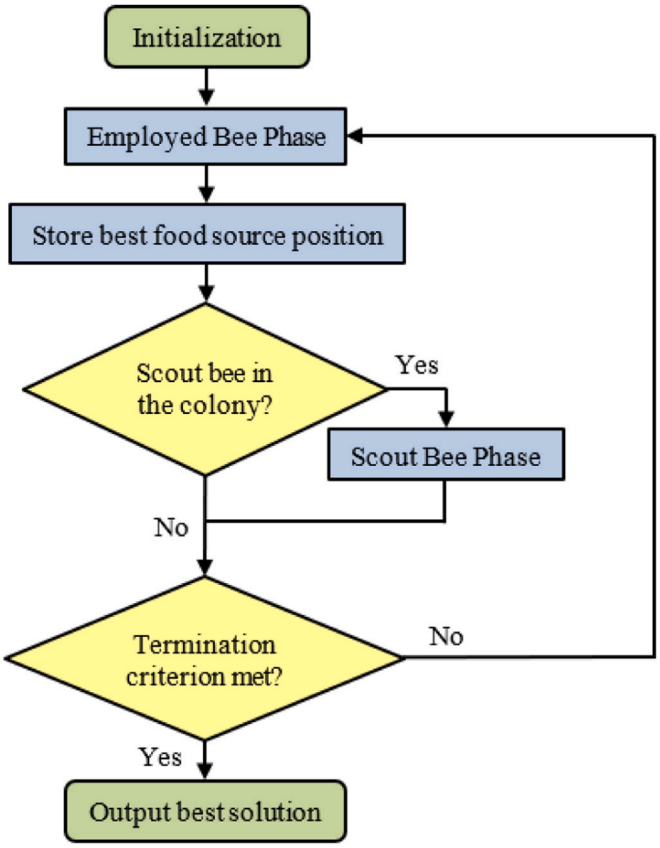

Fig. 4. The ABC algorithm flowchart.

2.1.3. Implementation steps of the ABC algorithm

The main steps of the ABC algorithm include initialization, determining the positions of worker and searcher bees on food sources in each iteration, and sending leading bees to search for new food sources until a desired state is reached. The implementation steps of this algorithm are as follows [62]:

1. Initialize the food sources.
2. Move worker bees towards food sources and determine nearby food sources.
3. Identify a new food source named V_i and substitute X_i if the nectar amount of the new source V_i (fitness value) proves superior to the existing source X_i.

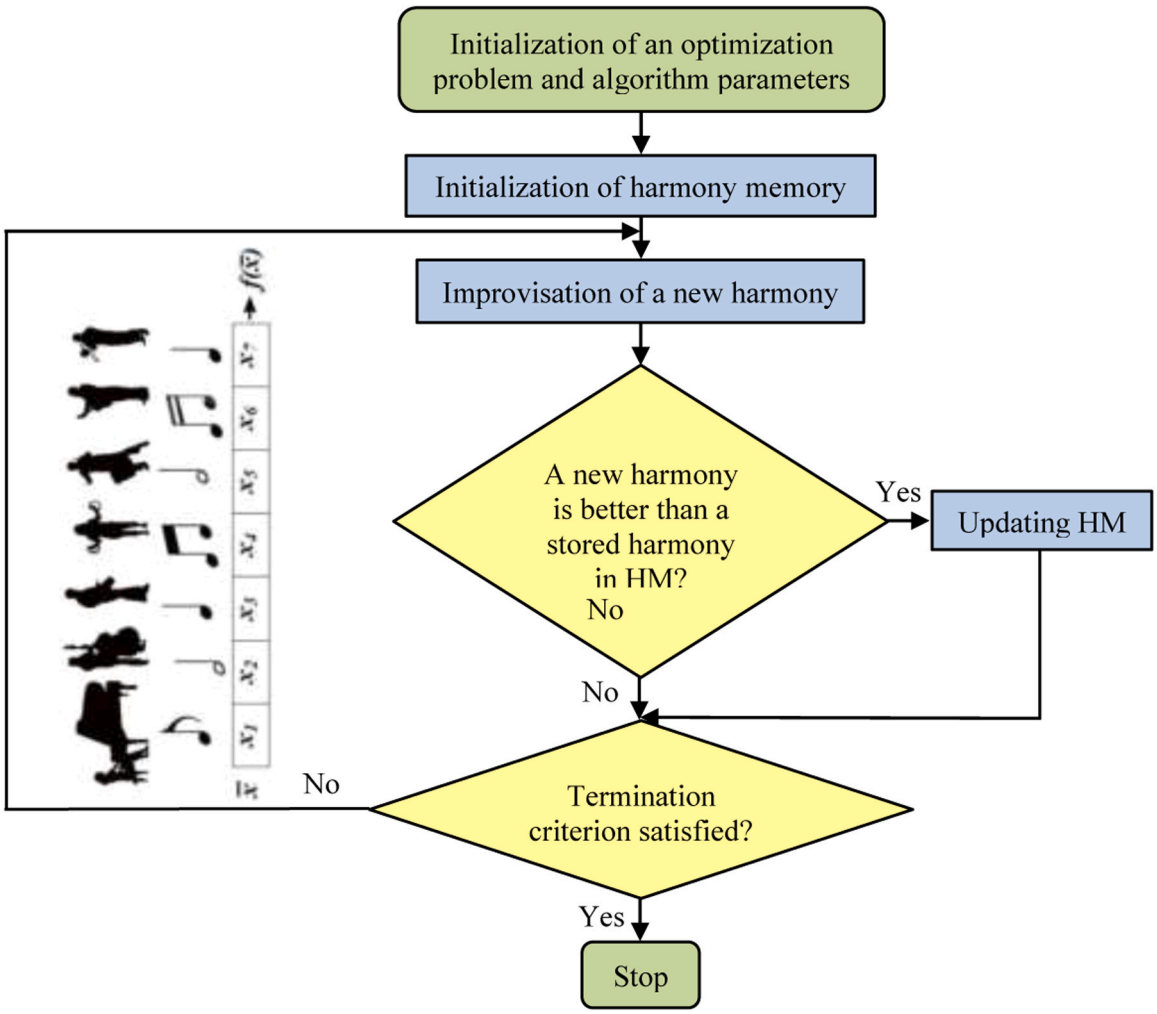

Fig. 5. The HS algorithm flowchart.

4. In the fourth step of the process, observe bees as they navigate towards food sources, and subsequently, create new neighbors by following the previously outlined steps in step 2.
5. If an improved food source is not discovered in the proximity after multiple attempts, a scout bee randomly picks a primary food source.
6. Iteratively execute steps 2 to 5 until an optimal solution is achieved.

Drawing upon the previously provided descriptions and the step-by-step implementation of the algorithm, the flowchart of the ABC algorithm is depicted in Fig. 4.

2.2. Harmony search (HS) algorithm

In 2001, Geem, Kim [63] introduced the HS algorithm, inspired by the way musicians generate harmonious melodies. Harmony in music refers to the combination of different notes that result in a melodic and pleasing composition. The goal of finding harmony in music aligns with the objective of finding optimal solutions to optimization problems. The HS algorithm has gained popularity in solving various problems due to its simplicity, low computational requirements, applicability to both discrete and continuous optimization problems, and ease of implementation [64,65].

The main steps of the HS algorithm for achieving the best (optimal) solution are described in the following:

Step 1: Problem Description and Algorithm Parameters.

In this step, the optimization problem is defined.

The algorithm's effectiveness hinges on a set of critical parameters. The upper and lower bounds for decision variables (x_{iu} and x_{iL}) play a pivotal role in defining the search space limitations. Additionally, the maximum number of iterations (k) dictates the runtime, while harmony memory size (HMS) determines the capacity for storing solutions. The step adjustment rate (PAR) guides the exploration of potential solutions, while the harmony memory check rate (HMCR) governs the acceptance of new solutions into the memory. Bandwidth (bw) contributes to pitch adjustment. These parameters collectively sculpt the algorithm's behavior, steering it through the solution space and enabling it to converge towards optimal outcomes within specified constraints.

Step 2: Random Generation of Initial Harmony Memory (HM).

The HM, serving as a collection of potential solutions, is randomly generated within the range of feasible values for the decision variables.

Step 3: Modification of New Harmony.

A new harmony vector $x^{new} = (x_1^{new}, x_2^{new}, \ldots, x_n^{new},)$ is created using three mechanisms: consideration of HM, random selection, and pitch adjustment rate [63,66,67]. For the new harmony vector, the decision variables are randomly selected from a range of values, and this choice is influenced by the probability of HMCR-1 [68].

HMCR represents the rate at which values are chosen from the HM, ranging from 0 to 1. The residual probability, denoted as (HMCR-1), signifies the proportion at which values are chosen randomly from the feasible range. This aspect of the algorithm introduces an element of randomness to the decision-making process, allowing for a diversified exploration of the solution space. As the algorithm progresses, this

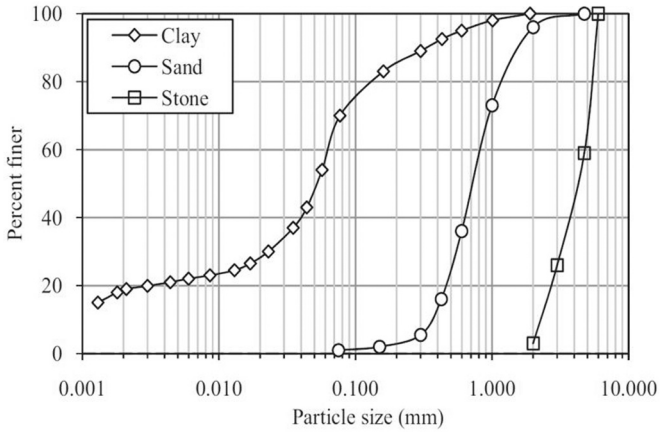

Fig. 6. The curves that represent the particle size distribution for stone, clay, and sand aggregate [71,72].

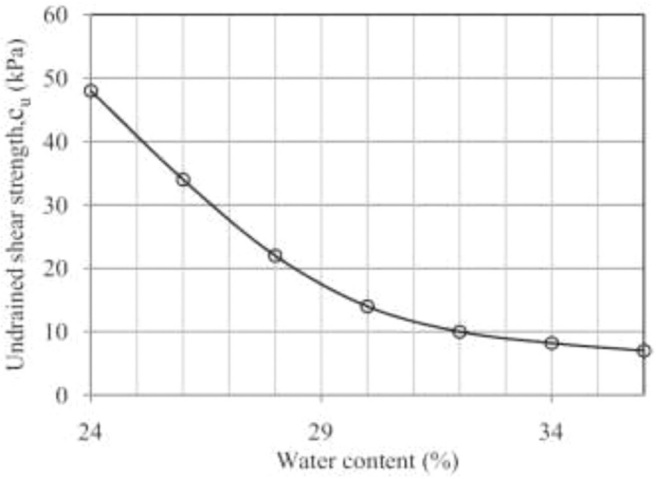

Fig. 7. The values of c_u vs water content [71,72].

randomized selection, guided by the remaining probability after considering the HMCR, contributes to the diversity of solutions, potentially enhancing the algorithm's ability to navigate and discover optimal outcomes in complex and dynamic problem landscapes. The decision variable values are then checked against the memory, and if the adjustment criteria are met with PAR probability, the variable is adjusted.

Step 4: Update HM.

After generating the new harmony vector, expressed as $x^{new} = (x_1^{new}, x_2^{new},\ldots,x_n^{new},)$, the HM undergoes an update in Step 4. If the performance of the new harmony vector outperforms the worst harmony stored in memory, the associated goal function value is replaced, and the worst harmony is expunged from memory. This dynamic updating mechanism ensures that the Harmony Memory retains high-performing solutions, optimizing the algorithm's ability to converge towards superior outcomes. By continually refreshing the memory with improved solutions, the algorithm adapts and refines its search space, contributing to its efficiency in solving complex optimization problems.

Step 5: Iterate Steps 3 and 4 Until the Stopping Condition (k) is Reached.

The third and fourth phases are repeated until the specified halting condition, determined by the maximum number of iterations (k), is met.

The flowchart of the HS method is represented in Fig. 5, which is based on the description that was received before.

3. Experimental technique

3.1. Materials used

Stone aggregate, geogrid, clay, and sand were some of the components that were utilized in the experimental inquiry with a variety of materials. In Fig. 6, the gradation curves of the aggregates consisting of stone, clay, and sand are depicted. The clay was used as the foundation for the construction of the stone columns, while the sand served as a protective layer for the soft clay that was supported and reinforced by the stone columns. In accordance with ASTM D4318 [69], the clay exhibited the following index properties: plasticity index: 21%, plastic limit: 22%, and liquid limit: 43%. The System of Unified Soil Classification classified this specific soil as inorganic clay with restricted flexibility (CL) [70]. This classification was made according to the soil's characteristics.

To assess undrained shear strength (cu) at specific consistency, Unconfined Compressive Strength (UCS) tests were conducted on soil samples with varied water contents. These tests involved subjecting soil samples to unconfined compressive forces, providing insights into their resistance and undrained shear strength characteristics at different moisture levels. This systematic approach offers valuable data for understanding soil behavior under diverse conditions, essential for geotechnical analyses and engineering applications. A representation of the link between water content and cu can be found in Fig. 7. Over the course of all the experiments, the water content of the soft clay remained unchanged at roughly 32%, which led to a bulk density (γ) of 18.15 kilonewtons per cubic measurement. After performing the calculations, it was found that the cu value was 10 kPa, which is equivalent to a water content of 32%.

Table 1
The geogrid reinforcement requirements, according to ASTM D6637 [73].

Parameter	Value
Strength at ultimate tension (kN/m)	20
Strain with maximum force (%)	16
Shear stiffness at ultimate strain [J (kN/m)]	125
Mass (g/m^2)	190
Mesh aperture size (mm×mm)	10 × 10
Thickness (mm)	1.5

In order to construct the stone columns, crushed stone aggregates were utilized. These aggregates displayed a coefficient of homogeneity of 2.13. In terms of grading, these aggregates were not very good; their particle sizes ranged from 2 to 6 millimeters. Seventy percent was the compression density that was brought about by the stone aggregates. The measurement for the angle of direct shear friction yielded 46 degrees, and the bulk density of the stone aggregate was determined to be 15.8 kN/m3 at a relative density of 70%.

The homogeneity and curvature factors of the sand that was utilized for the sand blanket or sand bed were 3.4 and 0.7, respectively, and it was able to pass through a sieve with a diameter of 4.75 millimeters. For each and every test, the sand bed was created with a relative density of seventy percent. Derived from the triaxial CD test results, the shear strength characteristics of the sand samples at a relative density of 70% indicated a cohesion of 0 and an internal friction angle of 42 degrees. According to the measurements, the bulk density was 16.7 kN/m3 when the relative density was 70%. A layer of high-density polyethylene biaxial geogrid was applied in order to strengthen the composition of the sand bed. The specifications for geogrid reinforcement are presented in Table 1 [73], which is in compliance with ASTM D6637.

3.2. Test setup

The test setup utilized a square tank measuring 1000 millimeters in length, 1000 millimeters in width, and 1000 millimeters in height (as depicted in Fig. 8a). To minimize friction and prevent water loss, a

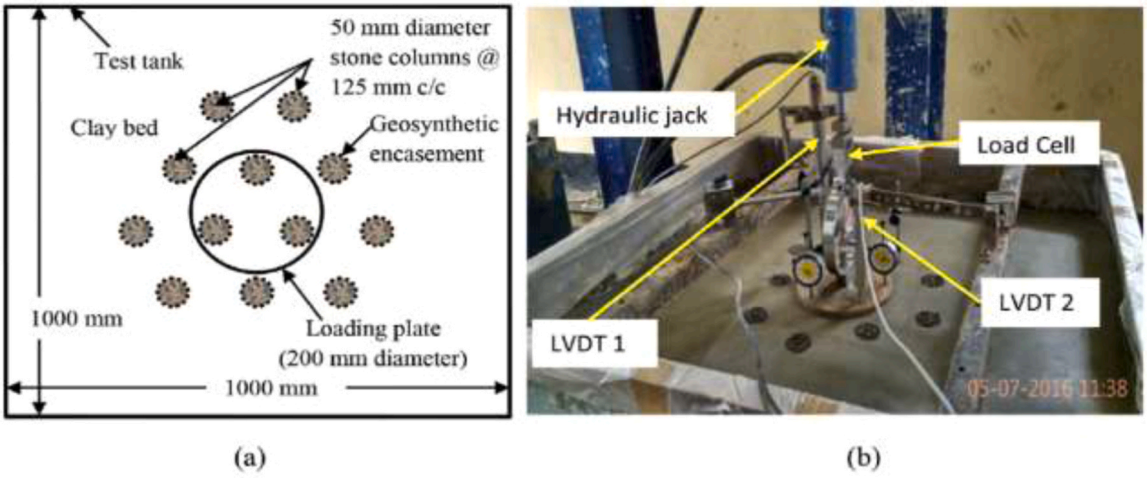

Fig. 8. : Load tests were conducted on a group of stone columns, with (a) illustrating the layout of vertically encased stone columns, and (b) providing a visual representation of the experimental setup [71].

robust polythene layer was initially applied to the tank's inner walls. The subsequent process involved filling the tank with soft clay in 100-millimeter thick layers. This stepwise addition of clay facilitated controlled and systematic testing, ensuring precise conditions for studying the behavior of soft clay. The carefully designed experimental setup aimed to provide insights into the interactions and characteristics of the soft clay under specified conditions. In each and every one of the experiments, the density of the clay and the amount of water it contained remained unchanged. To achieve the desired consistency, water with a water content of 32% was thoroughly mixed with the appropriate weight of dried clay for each 100 mm layer. The experiment involved the construction of stone columns within a clay substrate, conducted by the research group. The columns were formed using a steel pipe with an open end, having inner and outer diameters of 48.5 mm and 50 mm, respectively. This specific type of pipe was selected for its suitability in establishing columns. The pipes were strategically placed at specific locations within the clay substrate. The process involved the use of spiral steel augers to remove soil from the clay bed, with clay being extracted in increments of fifty millimeters throughout the operation. To facilitate the removal of clay, a thin layer of oil film was applied to the inner surface of the steel tube. This technique aimed to reduce friction and ease the extraction process. The weight of the required stone for the columns was determined based on the volume of the hole created during soil removal. Importantly, the relative density of the stone was maintained at a constant 70% throughout all the series of tests. The construction process followed a systematic approach to ensure precision and effectiveness. The open-ended steel pipes were inserted into the clay substrate, and the spiral steel augers efficiently removed soil in increments of fifty millimeters. The application of an oil film to the inner surface of the steel tube reduced friction, allowing for smoother clay removal. Crucially, the weight of the stone used in the columns was carefully calculated based on the volume of the hole left by the extracted clay. This method ensured that the relative density of the stone remained constant at the desired 70% level across all tested series. Maintaining a consistent relative density is crucial for standardizing the experimental conditions and ensuring reliable and comparable results. In order to fill each segment of the column, the stone material was first separated into five equal portions and then poured into each section. The next step was to ensure that the material was compacted uniformly up to a height of fifty millimeters by employing steel tampers with diameters of fifteen millimeters and twenty-five millimeters, respectively. An illustration of the configuration of the stone columns can be found in Fig. 8b. Fig. 8a is a graphical representation of the experimental setup, which shows the three stone columns that are located in the center of the experiment. In

Table 2
Overview of the Experiment [72].

Testing series	Reinforcement style	Specifics of the parameters examined
1	Clay+ SC	d_{sc}= 50 mm, L= 300 mm, S= 2.5 ×d_{sc}
2	USB+ Clay+ SC	VP: t/D= 0.1, 0.5, 0.4, 0.3, 0.15, 0.2 CP: S/d_{sc}= 2.5, L/d_{sc}= 6
3	GRSB+ Clay+ SC	VP: t/D= 0.3, 0.1, 0.2 CP: d/D= 4, S/d_{sc}= 2.5, L/d_{sc}= 6
4	GRSB+ Clay+ SC	VP: d/D= 1.5, 2.0, 2.5, 3.0 CP: S/d_{sc}= 2.5, L/d_{sc}= 6, t/D= 0.2
5	GRSB+ Clay+ SC	VP: L/d_{sc} = 2.0, 4.0, 8.0 CP: S/d_{sc}= 2.5, d/D= 2.5, t/D= 0.2

Variable parameters: VP, Constant parameters: CP.

accordance with the requirements of IS 15284 Part I [74], a group test consisting of three columns necessary a minimum of twelve columns in order to imitate the field condition of soil compaction in the intervening area.

In the case of GRSB [75], arrangement of columns followed a triangular pattern, ensuring an optimal distribution with a separation distance set at 2.5 times the diameter of each column. Achieving a specific gravity corresponding to 70% relative density involved the use of a circular steel hammer, effectively compacting dry sand layers. To enhance the setup, a 5-millimeter layer of sand was uniformly applied atop the clay base. The geogrid was strategically positioned in a circular configuration at the central point of the stone column array. Precise adjustments to the sand bed thickness were made to meet the specified requirements. As a stable foundation, a robust steel plate with a diameter (D) of 200 millimeters and a thickness of 15 millimeters served as the base. This footing was consistently positioned at the center of the tank in each test, ensuring uniformity in the experimental setup.

3.3. Test procedure

In the course of each test, a load was applied to the footing by means of a hydraulic jack. The footing was fitted with a load cell that was able to measure loads of up to one hundred kilonewtons. The load was gradually raised while remaining constant until the footing reached a stable state, at which point there was no discernible change in settlement that was greater than 0.02 mm/min. Short-term loading tests were conducted for each trial, and settlement measurements were obtained using linear variable differential transformers (LVDTs) installed at the footings. Two LVDTs were employed, with a minimum measurement resolution of 0.01 mm. In order to record the information that was obtained from the load cells and LVDTs, a portable data gathering

Table 3
Part of input and output data for modeling by ABC and HS algorithm [71].

Input Number	L/d_{sc}	s/D (%)	d/D	t/D	q_u(KPa)	Output q_{rs} (KPa)
1	6.00	0.84	0.00	0.00	7.09	11.39
2	6.00	1.72	0.00	0.00	15.56	23.10
3	6.00	2.60	0.00	0.00	23.26	33.81
4	6.00	3.65	0.00	0.00	30.77	44.57
5	6.00	4.98	0.00	0.00	37.28	53.39
6	6.00	6.41	0.00	0.00	41.84	60.63
7	6.00	8.24	0.00	0.00	45.35	66.70
8	6.00	10.22	0.00	0.00	47.86	73.48
9	6.00	12.21	0.00	0.00	49.83	78.46
10	6.00	14.20	0.00	0.00	51.36	83.56
11	6.00	16.19	0.00	0.00	52.54	86.54
12	6.00	18.18	0.00	0.00	53.27	89.60
13	6.00	20.00	0.00	0.00	53.82	92.11
14	6.00	0.65	0.00	0.10	5.50	11.50
15	6.00	1.34	0.00	0. 10	12.00	23.18
16	6.00	1.96	0.00	0. 10	17.77	33.64
17	6.00	2.70	0.00	0. 10	24.08	45.17
18	6.00	3.59	0.00	0. 10	30.38	56.57
19	6.00	4.85	0.00	0. 10	36.73	67.52
20	6.00	6.42	0.00	0. 10	41.87	77.16

Table 4
Input and output data set statistics description.

Statistical index	q_u (kPa)	s/D (%)	t/D	d/D	L/d_{sc}	q_{rs} (kPa)
Minimum	4.210	0.500	0.000	0.000	2.000	11.390
Maximum	53.820	20.000	0.500	4.000	8.000	309.760
Mean	38.198	38.198	0.216	1.596	5.817	133.005
Standard deviation	15.723	6.420	0.114	1.562	1.085	77.352
Range	49.610	19.500	0.500	4.000	6000	298.370

equipment that had twelve channels was utilized. Before the tests were carried out, each instrument was calibrated in the appropriate manner. Every test was carried out with the load being applied in a continuous manner until the settlement reached twenty percent of the footing diameter. After the stress test was finished, the three central stone columns were filled with a thin cement slurry so that their bulging and lateral deformations could be evaluated without causing any damage to the columns. Table 2 contains a complete rundown of the experiments that were carried out for the purpose of this research.

4. Modeling and presentation of results

Due to the inherent complexity and uncertainties associated with geological parameters, traditional methods such as regression, experimental, numerical, and analytical approaches have limitations in accurately calculating the qrs. These methods fail to capture the intricate nonlinear behavior exhibited in various case studies. To overcome these challenges and achieve accurate predictions closely aligned with actual values, intelligent methods offer a suitable alternative. By utilizing intelligent methods, a comprehensive model can be developed to determine the qrs under different parameters and characteristics. In this study, the ABC algorithm and HS method are employed to estimate the qrs.

Table 3 presents a portion of the 219 experimental data points collected in the present study. Key input parameters encompass the qrs of unreinforced soft clay (qu), the ratio of GRSB and USB thickness to base diameter (t/D), the ratio of the diameter of the geogrid-reinforced layers to the footing diameter (d/D), the ratio of stone column length to diameter (L/dsc), and the settlement-to-footing diameter ratio (s/D). The only output parameter considered is the qrs. For accurate estimation of the qrs, the data is randomly divided into two groups: 80% (175 data) for training the model and 20% (44 data) for evaluating the model's performance. The statistical features of both the input and output data

Table 5
Tuning parameters for the ABC.

Parameter	Value
Population Size	50
Maximum number of iterations	500
Acceleration Coefficient Upper Bound	1

Table 6
Tuning parameters for the HS.

Parameter	Value
Maximum number of iterations	6000
Number of New Harmonies	50
HM Size	60
bw	0.05
HMCR	0.9
PAR	0.19

are presented in Table 4.

To ensure accurate modeling results, the data in Table 3 is normalized within the range of [0,1] using Eq. (1):

$$X_n = [(X_{mea} - X_{\min})/(X_{\max} - X_{\min})] \quad (1)$$

In the equations, X_n represents the normalized values, X_{mea} represents the actual value, and X_{max} and X_{min} represent the maximum and minimum values, respectively.

After normalizing the training and test data, two nonlinear equations are formulated using MATLAB software to estimate the qrs through the ABC and HS optimization algorithms (Eq. (2)):

$$q_{rs} = (w_1 \times q_u) - (w_2 \times s/D) \times (w_3 \times (t/D)^{w_4}) - (w_5 \times d/D) - (w_6 \times L/d_{sc}) - w_7 \quad (2)$$

The weighting factors w_i are associated with the input parameters. To develop accurate estimation models for qrs using the ABC and HS algorithms, various setting parameters are determined by the user and presented in Tables 5 and 6, respectively.

Once the relationship and setting parameters are established, the MATLAB software is used to implement the coding for both algorithms. The prediction coefficients for Eq. (2) to estimate the qrs are obtained as shown in Eqs. (3) and (4) for the ABC and HS algorithms, respectively.

$$q_{rs} = (0.7941 \times q_u) - (0.1407 \times s/D) \times \Big(0.1194 \times (t/D)^{0.0011}\Big) - \Big(\big(-0.3115\big) \times d/D\Big) - \Big(\big(-0.1880\big) \times L/d_{sc}\Big) - 0.2831 \quad (3)$$

$$q_{rs} = (0.9305 \times q_u) - (0.0901 \times s/D) \times \Big(0.0092 \times (t/D)^{0.0103}\Big) - \Big(\big(-0.7139\big) \times d/D\Big) - \Big(\big(-0.0915\big) \times L/d_{sc}\Big) - 0.5178 \quad (4)$$

5. Evaluation of models

After implementing the MATLAB code and adjusting parameters for the two algorithms mentioned above, several statistical indicators were used to validate and accurately predict the nonlinear relationships represented by Eqs. (3) and (4). These metrics encompass Variance Account For (VAF), Mean Square Error (MSE), Mean Absolute Percentage Error (MAPE), Squared Correlation Coefficient (R^2), and Root Mean Square Error (RMSE). High accuracy and low error in the model can be determined if the values of VAF and R^2 are close to one, and the values of MSE, RMSE, and MAPE are close to zero [76–84]. In such cases, the predicted values closely align with the actual values, indicating the

Table 7
Validation of predictive relationships using ABC and HS.

Algorithm type	Description	VAF	R^2	MAPE	MSE	RMSE
ABC algorithm	Train	0.93931	0.93532	0.00432	0.00327	0.05715
HS algorithm	Test	0.97086	0.97251	0.00133	$7.86 * 10^{-5}$	0.00883
	Train	0.94975	0.94034	0.00256	0.00115	0.03387
	Test	0.98917	0.98132	0.00083	$3 * 10^{-5}$	0.00551

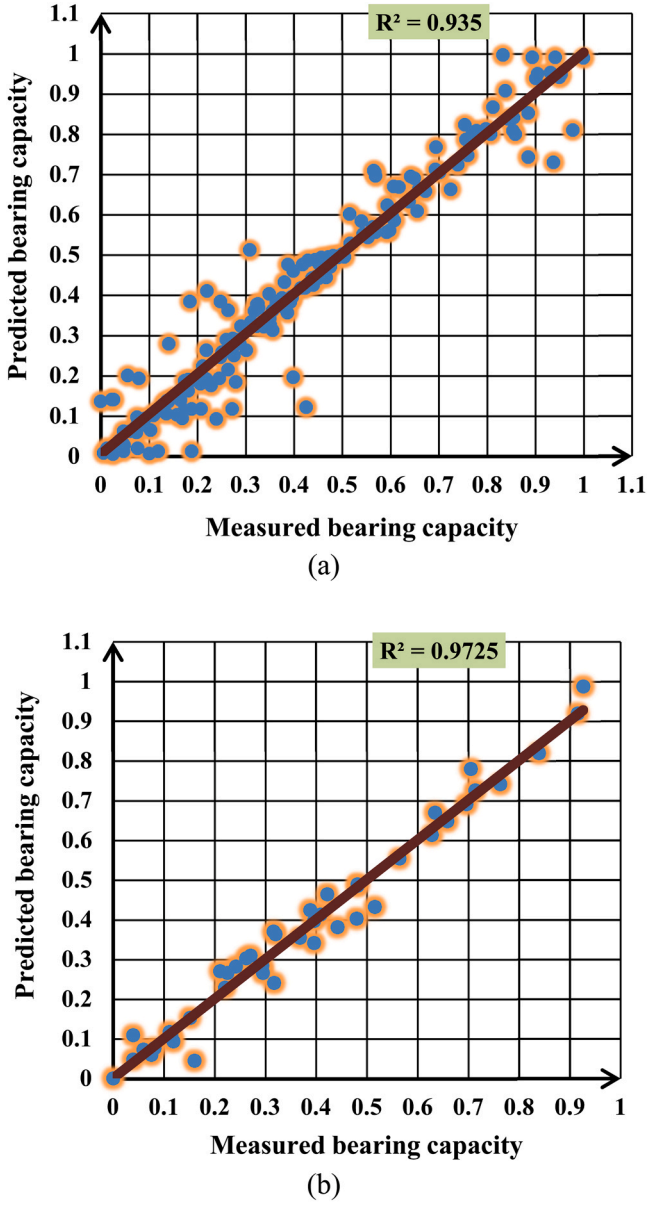

Fig. 9. Correlation between predicted and measured qrs using the ABC algorithm for (a) training data, (b) test data.

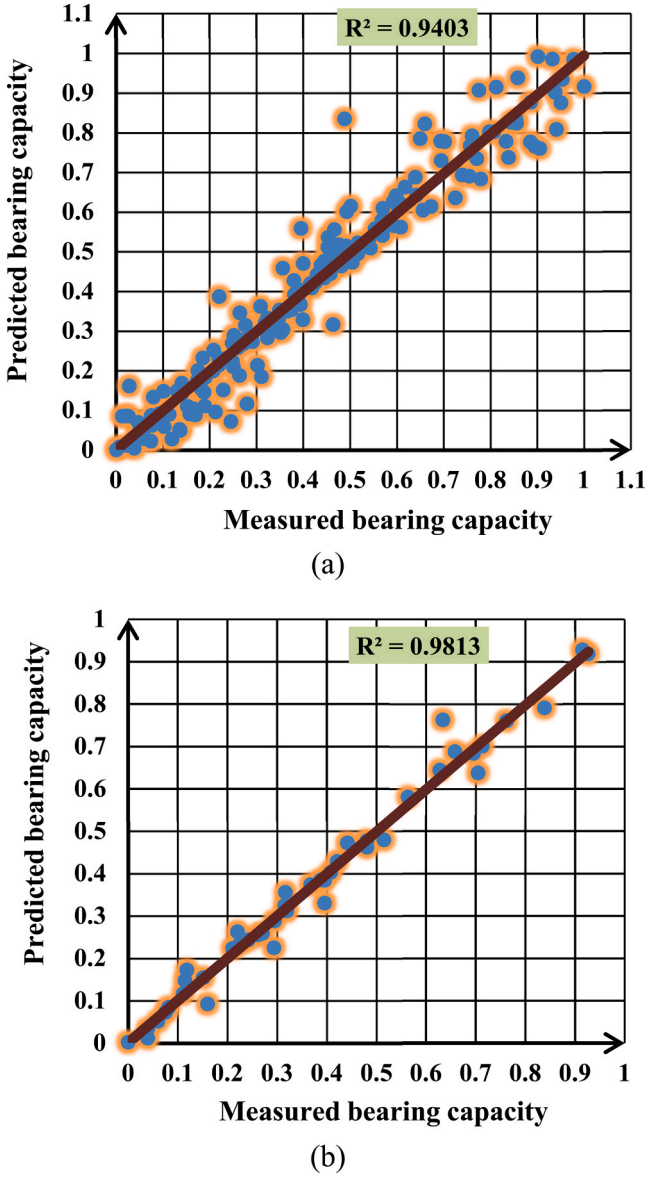

Fig. 10. : Correlation between predicted and measured qrs using the HS algorithm for (a) training data, (b) test data.

efficacy of the equation in predicting the qrs. The relationships for the VAF, R^2, MSE, RMSE, and MAPE indicators are defined as Eqs. (5) to (9) respectively,

$$VAF = \left[1 - \frac{\mathrm{var}(Y_{mea} - Y_{pre})}{\mathrm{var}(Y_{mea})}\right] \tag{5}$$

$$R^2 = 1 - \frac{\sum_{k=1}^{n} \left(Y_{mea} - Y_{pre}\right)^2}{\sum_{k=1}^{n} Y_{mea}^2 - \frac{\sum_{i=1}^{n} Y_{pre}^2}{n}} \tag{6}$$

$$MSE = \frac{1}{n} \sum_{i=1}^{n} \left(Y_{mea} - Y_{pre}\right)^2 \tag{7}$$

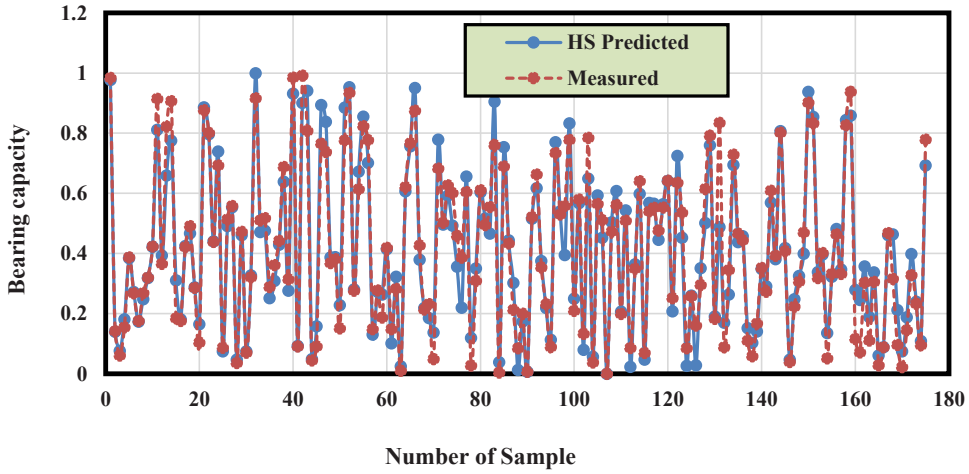

(a)

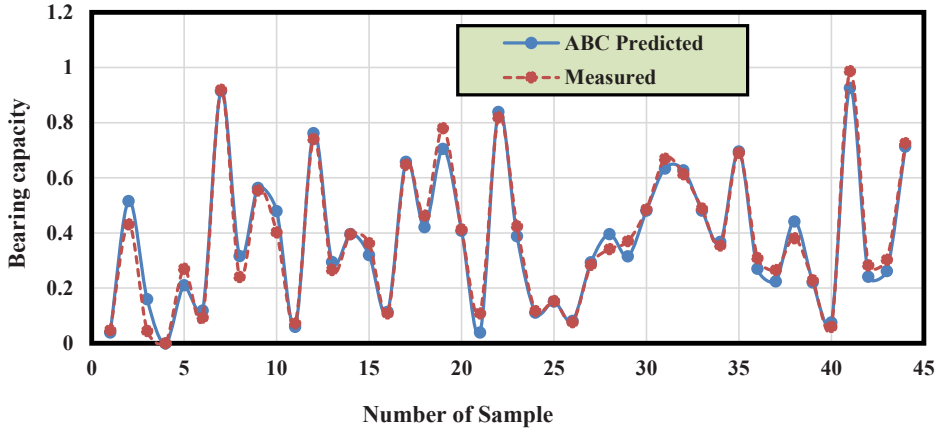

Fig. 11. : Measured vs predicted qrs using the ABC for (a) training data, (b) test data.

$$RMSE = \sqrt{\frac{1}{n}\sum_{i=1}^{n}\left(Y_{mea} - Y_{pre}\right)^2} \tag{8}$$

$$MAPE = \frac{1}{n}\sum_{i=1}^{n}\left|Y_{mea} - Y_{pre}\right| \tag{9}$$

where Y_{max} represents the measured values, Y_{pre} represents the predicted values, and n is the number of samples. The values of these indicators for the prediction models obtained from the ABC algorithm and HS algorithm, in both the training and testing phases, are presented in Table 7.

Measured and predicted qrs values obtained from the ABC and HS algorithms for both the training and testing datasets are shown in Figs. 9 and 10, respectively.

According to Table 7, the nonlinear prediction relationships obtained through the ABC and HS algorithms demonstrate good accuracy in estimating the qrs. Furthermore, the estimated values of the qrs by the A and HS models closely match the measured values for the 219 data points in both the training (175 data) and test (44 data) datasets. This indicates a minimal error in the created relationship, suggesting its effectiveness in predicting the actual values. Consequently, the relationships established by these algorithms can be employed to estimate the qrs in other case studies.

Furthermore, we conducted a comparative analysis of the findings presented in this study with those reported by Dadhich et al. [85] and Bong et al. This comparison is detailed in Table 8. As outlined in Table 8, our proposed methodologies encompass five distinct approaches: multivariate linear regression (MLR), SVR, random forest regression (RFR), ANN and DNN. The results obtained from our proposed methodologies were juxtaposed with those derived from the ABC and HS algorithms. Notably, our analysis reveals that the models utilizing the ABC and HS algorithms outperform the previously published models. Specifically, as delineated in Table 8, the HS model attains the highest predictive accuracy, with an R^2 value of 0.9813 and an RMSE of 0.00551.

6. Limitations and future works

This comprehensive study delved into the intricacies surrounding the accurate prediction of the qrs of reinforced stone columns, with a predominant focus on the geometrical parameters influencing their structural integrity. However, it is imperative to acknowledge the multifaceted nature of this subject matter, as numerous other factors, including soil and rock geotechnical parameters, play pivotal roles in determining the robustness of such foundational elements. Therefore, this discourse aims to delve deeper into the limitations encountered in the current study and outline prospective avenues for future research endeavors.

Diverse Factors Influencing qrs: While the present study meticulously scrutinized the geometrical attributes of reinforced stone columns, it is imperative to underscore the significance of incorporating a broader spectrum of factors into the predictive framework. Soil and rock geotechnical parameters, encompassing aspects such as shear strength,

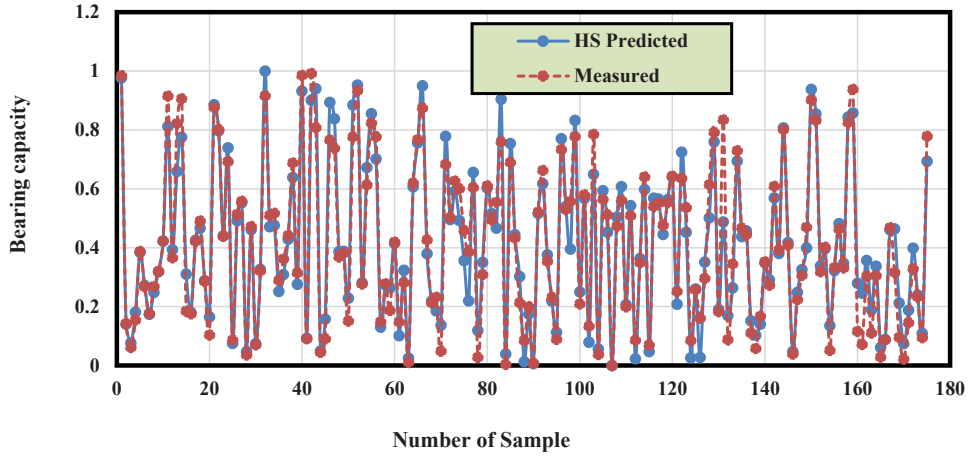

(a)

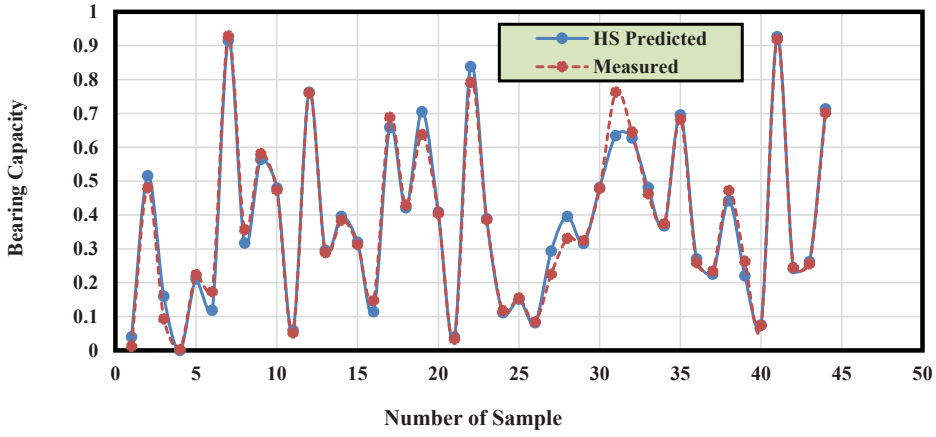

(b)

Fig. 12. : Measured vs predicted qrs using the HS for (a) training data, (b) test data.

Table 8
Comparison of performance of the proposed models and previously presented model.

Models		R^2	RMSE
ABC algorithm	Training	0.9353	0.05715
(Proposed in this study)	Testing	0.9725	0.00883
HS algorithm	Training	0.9403	0.03387
(Proposed in this study)	Testing	0.9813	0.00551
MLR model[85]	Training	0.9603	58.87
	Testing	0.8135	136.67
SVR model[85]	Training	0.9341	75.02
	Testing	0.8310	174.43
RFR model[85]	Training	0.9801	52.74
	Testing	0.9801	44.43
ANN model[85]	Training	0.8980	104.83
	Testing	0.9558	78.54
DNN model[86]	Training	0.9241	-
	Testing	0.9306	
Multivariate linear regression model[86]	Training	0.9371	82.74
	Testing	0.9552	101.36

cohesion, and angle of internal friction, wield profound influence over the bearing capacity of these structural elements. Neglecting to account for these intrinsic soil and rock characteristics could potentially undermine the accuracy and reliability of predictive models, thus underscoring the necessity for their inclusion in future research endeavors.

Integration of Intelligent Algorithms and Modeling Techniques: In addressing the imperative need for enhanced prediction accuracy, future research endeavors hold immense promise by integrating cutting-edge intelligent algorithms and advanced modeling techniques. The utilization of algorithms such as ABC and HS in tandem with sophisticated models like ANN, SVM, ANFIS and SVR presents a compelling avenue for refining predictive capabilities. By harnessing the computational prowess of these algorithms and leveraging the vast repository of data at our disposal, researchers can endeavor to unravel the intricate interplay between various geomechanical properties of rock and soil and the geometric parameters of reinforced stone columns.

Challenges in Model Applicability: A notable limitation inherent in the methodology employed in the current study pertains to the restricted applicability of the constructed relationships. The findings derived from this study may be inherently tied to the specific geological and geotechnical characteristics of the study area, thereby limiting their generalizability to broader contexts. Consequently, when extrapolating these findings to disparate geological settings or distinct study areas, researchers must exercise prudence and vigilance. Should the geotechnical parameters of a given locale diverge significantly from those encapsulated within the study framework, the viability of applying the established models becomes questionable. Thus, the onus falls on future research endeavors to undertake rigorous validation exercises across diverse geological contexts to ascertain the robustness and reliability of

predictive models.

Exploring Alternative Optimization Strategies: In charting the trajectory for future research initiatives, it is imperative to explore alternative optimization strategies and refine existing models to confront the myriad complexities and uncertainties pervasive within the field. By broadening the scope to encompass a diverse array of optimization algorithms, researchers can glean invaluable insights into their efficacy in predicting the bearing capacity of reinforced stone columns. Furthermore, refining existing models to encapsulate additional complexities, such as dynamic loading conditions and temporal variations, holds immense potential in fortifying the resilience and adaptability of predictive frameworks.

In summation, while the current study has made commendable strides towards unraveling the complexities surrounding the prediction of bearing capacity in reinforced stone columns, it is evident that significant avenues for further exploration remain. By transcending the confines of conventional methodologies and embracing a multidisciplinary approach, researchers can aspire to unlock new frontiers in predictive accuracy and reliability. Thus, through concerted efforts aimed at integrating advanced modeling techniques, harnessing the computational prowess of intelligent algorithms, and undertaking rigorous validation exercises, the field of geotechnical engineering stands poised to usher in a new era of innovation and discovery in the realm of foundation design and structural integrity.

7. Discussion and conclusion

The accurate prediction of qrs poses a significant challenge in geotechnical engineering due to the complexity and variability of soil and rock parameters. In this study, we investigated the application of two intelligent optimization algorithms, namely HS and ABC, to estimate qrs. By utilizing these algorithms, we aimed to improve the accuracy and efficiency of qrs predictions while considering uncertainties. The dataset used for our analysis consisted of 219 data points, encompassing various input parameters such as d/D, L/dsc, qu, GRSB and t/D, and s/D. We randomly divided the data into a training phase, which accounted for 80% (175 data points), and a testing phase, comprising the remaining 20% (44 data points) used for validation and evaluation. After constructing the models using the ABC and HS algorithms and implementing MATLAB coding, we employed several statistical indicators, including VAF, R^2, MSE, RMSE, and MAPE, to examine the performance of the developed models. Based on the findings, it was clear that both algorithms were successful in achieving a high level of accuracy, as they nearly matched the real values of qrs. This demonstrates that the intelligent optimization techniques are effective in providing an accurate estimation of the qrs of stone columns reinforced with geogrid. Comparing the performance of traditional methods with intelligent optimization algorithms highlighted the advantages of the latter in terms of accuracy and efficiency. Traditional methods, such as regression, experimental, analytical, and numerical approaches, often lack precision and tend to deviate from the actual values of qrs. Conversely, the HS and ABC algorithms provide reliable and consistent predictions, offering a significant improvement over conventional approaches. The findings of this study have important implications for geotechnical engineering practice. Accurately predicting qrs is crucial for the design and construction of structures supported by geogrid-reinforced stone columns. The use of intelligent optimization algorithms, such as HS and ABC, can enhance the reliability of these predictions, reducing the risk of costly errors and ensuring the safety and stability of geotechnical projects. Furthermore, the proposed limit state function developed in this study can be generalized to various regions, considering geological and geotechnical conditions. This broad applicability further enhances the practical significance of the developed models. In conclusion, their research showcases the effectiveness of the HS and ABC optimization algorithms in precisely forecasting the qrs of geogrid-reinforced stone columns. These intelligent techniques yield notable enhancements in accuracy and efficiency when compared to conventional methods. The resultant models offer a dependable means for estimating qrs, thereby contributing to the advancement of design and construction practices within the field of geotechnical engineering.

CRediT authorship contribution statement

Hadi Fattahi: Writing – review & editing, Writing – original draft, Supervision, Software, Methodology, Conceptualization. **Hossein Ghaedi:** Writing – review & editing, Writing – original draft, Methodology. **Farshad Malekmahmoodi:** Writing – review & editing, Writing – original draft, Methodology. **Danial Jahed Armaghani:** Writing – review & editing, Writing – original draft, Conceptualization, Supervision.

Declaration of Competing Interest

The authors declare that they have no known competing financial interests or personal relationships that could have appeared to influence the work reported in this paper.

Data Availability

To reproduce the simulations in the present study, the corresponding files can be found in [71].

References

[1] Gniel J, Bouazza A. Improvement of soft soils using geogrid encased stone columns. Geotext Geomembr 2009;27(3):167–75.
[2] Hosseinpour I, Almeida MSS, Riccio M. Full-scale load test and finite-element analysis of soft ground improved by geotextile-encased granular columns. Geosynth Int 2015;22(6):428–38.
[3] Fattah MY, Zabar BS, Hassan HA. Experimental analysis of embankment on ordinary and encased stone columns. Int J Geomech 2016;16(4):04015102.
[4] Zhang Y, Li T, Wang Y. Theoretical elastic solutions for foundations improved by geosynthetic-encased columns. Geosynth Int 2011;18(1):12–20.
[5] Almeida M, Hosseinpour I, Riccio M. Performance of a geosynthetic-encased column (GEC) in soft ground: numerical and analytical studies. Geosynth Int 2013;20(4):252–62.
[6] Almeida MS, et al. Behavior of geotextile-encased granular columns supporting test embankment on soft deposit. J Geotech Geoenviron Eng 2015;141(3):04014116.
[7] Mohapatra SR, Rajagopal K, Sharma J. Direct shear tests on geosynthetic-encased granular columns. Geotext Geomembr 2016;44(3):396–405.
[8] Castro J. Groups of encased stone columns: influence of column length and arrangement. Geotext Geomembr 2017;45(2):68–80.
[9] Gu M, et al. Effects of geogrid encasement on lateral and vertical deformations of stone columns in model tests. Geosynth Int 2016;23(2):100–12.
[10] Ghazavi M, Afshar JN. Bearing capacity of geosynthetic encased stone columns. Geotext Geomembr 2013;38:26–36.
[11] KEMPFERT, H., Geotextile-Encased Columns (GEC) for Foundation of a Dike on Very Soft Soils.
[12] Ali K, Shahu J, Sharma K. Model tests on geosynthetic-reinforced stone columns: a comparative study. Geosynth Int 2012;19(4):292–305.
[13] Wu C-S, Hong Y-S. Laboratory tests on geosynthetic-encapsulated sand columns. Geotext Geomembr 2009;27(2):107–20.
[14] Poorooshasb H, Meyerhof G. Analysis of behavior of stone columns and lime columns. Comput Geotech 1997;20(1):47–70.
[15] Tang L, et al. Numerical study on ground improvement for liquefaction mitigation using stone columns encased with geosynthetics. Geotext Geomembr 2015;43(2):190–5.
[16] Ambily A, Gandhi SR. Behavior of stone columns based on experimental and FEM analysis. J Geotech Geoenviron Eng 2007;133(4):405–15.
[17] Bouassida M, Jellali B, Porbaha A. Limit analysis of rigid foundations on floating columns. Int J Geomech 2009;9(3):89–101.
[18] Özkul ZH, Baykal G. Shear behavior of compacted rubber fiber-clay composite in drained and undrained loading. J Geotech Geoenviron Eng 2007;133(7):767–81.
[19] Lee J, Pande G. Analysis of stone-column reinforced foundations. Int J Numer Anal Methods Geomech 1998;22(12):1001–20.
[20] Murugesan S, Rajagopal K. Geosynthetic-encased stone columns: numerical evaluation. Geotext Geomembr 2006;24(6):349–58.
[21] Lo S, Zhang R, Mak J. Geosynthetic-encased stone columns in soft clay: a numerical study. Geotext Geomembr 2010;28(3):292–302.
[22] Arulrajah A, et al. Ground improvement techniques for railway embankments. Proc Inst Civ Eng-Ground Improv 2009;162(1):3–14.
[23] Mehrannia N, Nazariafshar J, Kalantary F. Experimental investigation on the bearing capacity of stone columns with granular blankets. Geotech Geol Eng 2018;36(1):209–22.

[24] Andreou P, Papadopoulos V. Factors affecting the settlement estimation of stone column reinforced soils. Geotech Geol Eng 2014;32(5):1175–85.
[25] Xu F, et al. Laboratory and numerical analysis of geogrid encased stone columns. Measurement 2021;169:108369.
[26] Bazzazian Bonab S, et al. Experimental studies on single reinforced stone columns with various positions of geotextile. Innov Infrastruct Solut 2020;5(3):1–12.
[27] Thakur A, Rawat S, Gupta AK. Experimental and numerical modelling of group of geosynthetic-encased stone columns. Innov Infrastruct Solut 2021;6(1):1–17.
[28] Nasiri M, Hajiazizi M. Performance of reinforced stone column using geotextile & geogrid encasements in triaxial Test. Sharif J Civ Eng 2021;37(2.1):131–7.
[29] Hataf N, Nabipour N, Sadr A. Experimental and numerical study on the bearing capacity of encased stone columns. Int J Geo-Eng 2020;11(1):1–19.
[30] Das M, Dey AK. An innovative approach to increase the bearing capacity of stone columns. *Indian Geotech Conf Igc* 2016.
[31] Kardgar H. Investigation of the bearing capacity of foundations on encased stone columns using finite element method. Int J Integr Eng 2018;(1):**10**.
[32] Naderi E, Asakereh A, Dehghani M. Bearing capacity of strip footing on clay slope reinforced with stone columns. Arab J Sci Eng 2018;43(10):5559–72.
[33] Das M, Dey AK. Improvement of bearing capacity of stone columns: an analytical study. Ground Improvement and Reinforced Soil Structures. Springer,; 2022. p. 293–303.
[34] Pandey, B., S. Rajesh, and S. Chandra. Numerical Analysis of Soft Soil Reinforced with Geogrid Encased Stone Column. in Proceedings of the 7th Indian Young Geotechnical Engineers Conference. 2022. Springer.
[35] Das M, Dey AK. Use of soil cement bed in improvement of load carrying capacity of stone columns. Geotech Geol Eng 2020;38(6):6529–50.
[36] Shafiqu QSM, Al-Assady FAA. Numerical analysis of embankment supported by stone columns encased with geosynthetic material. J Sci Eng Appl 2019;1(3).
[37] Xie X, et al. Bearing behaviour of floating and end bearing encased stone columns with different encasement materials. Arab J Geosci 2022;15(8):1–12.
[38] Deb K, Samadhiya NK, Namdeo JB. Laboratory model studies on unreinforced and geogrid-reinforced sand bed over stone column-improved soft clay. Geotext Geomembr 2011;29(2):190–6.
[39] Li L-Y, Rajesh S, Chen J-F. Centrifuge model tests on the deformation behavior of geosynthetic-encased stone column supported embankment under undrained condition. Geotext Geomembr 2021;49(3):550–63.
[40] Mazumder T, Ayothiraman R. Numerical study on behaviour of encased stone columns with partial content of shredded tyre chips in soft clay bed. Int J Geosynth Ground Eng 2021;7(2):1–14.
[41] Kuo Y, et al. ANN-based model for predicting the bearing capacity of strip footing on multi-layered cohesive soil. Comput Geotech 2009;36(3):503–16.
[42] Momeni E, et al. Prediction of pile bearing capacity using a hybrid genetic algorithm-based ANN. Measurement 2014;57:122–31.
[43] Chik Z, Aljanabi QA. Intelligent prediction of settlement ratio for soft clay with stone columns using embankment improvement techniques. Neural Comput Appl 2014;25:73–82.
[44] Aljanabi QA, et al. Support vector regression-based model for prediction of behavior stone column parameters in soft clay under highway embankment. Neural Comput Appl 2018;30:2459–69.
[45] Mosallanezhad M, Moayedi H. Developing hybrid artificial neural network model for predicting uplift resistance of screw piles. Arab J Geosci 2017;10(22):479.
[46] Sahu, R., et al. Bearing capacity prediction of inclined loaded strip footing on reinforced sand by ANN. in Advances in Reinforced Soil Structures: Proceedings of the 1st GeoMEast International Congress and Exhibition, Egypt 2017 on Sustainable Civil Infrastructures 1. 2018. Springer.
[47] Moayedi H, Rezaei A. An artificial neural network approach for under-reamed piles subjected to uplift forces in dry sand. Neural Comput Appl 2019;31(2):327–36.
[48] Das M, Dey AK. Determination of bearing capacity of stone column with application of neuro-fuzzy system. KSCE J Civ Eng 2018;22:1677–83.
[49] Das M, Dey AK. Prediction of bearing capacity of stone columns placed in soft clay using SVR model. Arab J Sci Eng 2019;44(5):4681–91.
[50] Dey A, Debnath P. Empirical approach for bearing capacity prediction of geogrid-reinforced sand over vertically encased stone columns floating in soft clay using support vector regression. Neural Comput Appl 2020;32(10):6055–74.
[51] Mazumder T, Garg A. Comparison of accuracy in prediction of radial strain in stone columns using AI based models. Belt and Road Webinar Series on Geotechnics, Energy and Environment. Springer,; 2021. p. 209–22.
[52] Moayedi H, Hayati S. Applicability of a CPT-based neural network solution in predicting load-settlement responses of bored pile. Int J Geomech 2018;18(6):06018009.
[53] Jahed Armaghani D, et al. Developing a hybrid PSO–ANN model for estimating the ultimate bearing capacity of rock-socketed piles. Neural Comput Appl 2017;28:391–405.
[54] Bagińska M, Srokosz PE. The optimal ANN Model for predicting bearing capacity of shallow foundations trained on scarce data. KSCE J Civ Eng 2019;23:130–7.
[55] Sethy BP, et al. Prediction of ultimate bearing capacity of circular foundation on sand layer of limited thickness using artificial neural network. Int J Geotech Eng 2021;15(10):1252–67.
[56] Ardakani A, Dinarvand R, Namaei A. Ultimate shear resistance of silty sands improved by stone columns estimation using neural network and imperialist competitive algorithm. Geotech Geol Eng 2020;38(2):1485–96.
[57] Ghanizadeh AR, et al. Developing bearing capacity model for geogrid-reinforced stone columns improved soft clay utilizing MARS-EBS hybrid method. Transp Geotech 2023;38:100906.
[58] Gnananandarao T, Onyelowe KC, Murthy K. Experience in using sensitivity analysis and ANN for predicting the reinforced stone columns' bearing capacity sited in soft clays. in Artificial intelligence and machine learning in smart city planning. Elsevier,; 2023. p. 231–41.
[59] Lafifi B, Rouaiguia A, Soltani EA. A novel method for optimizing parameters influencing the bearing capacity of geosynthetic reinforced sand using RSM, ANN, and Multi-objective Genetic Algorithm. Stud Geotech Et Mech 2023;45(2):174–96.
[60] Zeini HA, et al. Prediction of the bearing capacity of composite grounds made of geogrid-reinforced sand over encased stone columns floating in soft soil using a white-box machine learning model. Appl Sci 2023;13(8):5131.
[61] Pham DT, et al. The bees algorithm—a novel tool for complex optimisation problems. in *Intelligent production machines and systems*. Elsevier,; 2006. p. 454–9.
[62] Karaboga, D., An idea based on honey bee swarm for numerical optimization. 2005, Technical report-tr06, Erciyes university, engineering faculty, computer ….
[63] Geem ZW, Kim JH, Loganathan GV. A new heuristic optimization algorithm: harmony search. simulation 2001;76(2):60–8.
[64] Lee KS, Geem ZW. A new meta-heuristic algorithm for continuous engineering optimization: harmony search theory and practice. Comput Methods Appl Mech Eng 2005;194(36-38):3902–33.
[65] Geem ZW. Global optimization using harmony search: Theoretical foundations and applications. Foundations of Computational Intelligence Volume 3. Springer,; 2009. p. 57–73.
[66] Alia OM, Mandava R. The variants of the harmony search algorithm: an overview. Artif Intell Rev 2011;36(1):49–68.
[67] Yuan X, et al. Hybrid parallel chaos optimization algorithm with harmony search algorithm. Appl Soft Comput 2014;17:12–22.
[68] Jaberipour M, Khorram E. Two improved harmony search algorithms for solving engineering optimization problems. Commun Nonlinear Sci Numer Simul 2010;15(11):3316–31.
[69] Soil, A.C.D.-o. and Rock, Standard test methods for liquid limit, plastic limit, and plasticity index of soils. 2010: ASTM international.
[70] ASTM, Standard practice for classification of soils for engineering purposes (unified soil classification system). D2487, West Conshohocken, PA, 2006.
[71] Debnath P, Dey AK. Prediction of bearing capacity of geogrid-reinforced stone columns using support vector regression. Int J Geomech 2018;18(2):04017147.
[72] Pandey B, Rajesh S, Chandra S. Numerical evaluation of geogrid-encased stone columns in soft soil under embankment loading. Geo-Congress 2020. Reston, VA: American Society of Civil Engineers,; 2020.
[73] ASTM, Standard test method for determining tensile properties of geogrid by single or multi-rib tensile methods. D6637, West Conshohocken, PA., 2001.
[74] Indian Standard, I., Design and construction for ground improvement-Guidelines. *Part 1: Stone columns*. IS, 2003. 15284: p. 267–290.
[75] Han J, Gabr M. Numerical analysis of geosynthetic-reinforced and pile-supported earth platforms over soft soil. J Geotech Geoenviron Eng 2002;128(1):44–53.
[76] Fattahi H, Hasanipanah M. An indirect measurement of rock tensile strength through optimized relevance vector regression models, a case study. Environ Earth Sci 2021;80(22):748.
[77] Fattahi H, Hasanipanah M, Zandy Ilghani N. Investigating correlation of physico-mechanical parameters and P-Wave velocity of rocks: a comparative intelligent study. J Min Environ 2021;12(3):863–75.
[78] Fattahi H. Analysis of rock mass boreability in mechanical tunneling using relevance vector regression optimized by dolphin echolocation algorithm. Int J Optim Civ Eng 2020;10(3):481–92.
[79] Fattahi H. A hybrid support vector regression with ant colony optimization algorithm in estimation of safety factor for circular failure slope. Int J Optim Civ Eng 2016;6(1):63–75.
[80] Fattahi H. A new approach for evaluation of seismic slope performance. Int J Optim Civ Eng 2020;10(2):261–75.
[81] Fattahi H, Babanouri N, Varmaziyari Z. A Monte Carlo simulation technique for assessment of earthquake-induced displacement of slopes. J Min Environ 2018;9(4):959–66.
[82] Fattahi H, Ghaedi H, Malekmahmoodi F. Prediction of rock drillability using gray wolf optimization and teaching–learning-based optimization techniques. Soft Comput 2024;28(1):461–76.
[83] Fattahi H, Nazari H, Molaghab A. Hybrid ANFIS with ant colony optimization algorithm for prediction of shear wave velocity from a carbonate reservoir in Iran. Int J Min Geo-Eng 2016;50(2):231–8.
[84] Fattahi H, Zandy Ilghani N. Hybrid wavelet transform with artificial neural network for forecasting of shear wave velocity from wireline log data: a case study. Environ Earth Sci 2021;80(1):5.
[85] Dadhich S, Sharma JK, Madhira M. Prediction of ultimate bearing capacity of aggregate pier reinforced clay using machine learning. Int J Geosynth Ground Eng 2021;7:1–16.
[86] Bong T, Kim S-R, Kim B-I. Prediction of ultimate bearing capacity of aggregate pier reinforced clay using multiple regression analysis and deep learning. Appl Sci 2020;10(13):4580.